MDPI

Article

Dimensioning Methodology of an Energy Storage System Based on Supercapacitors for Grid Code Compliance of a Wave Power Plant

Gustavo Navarro [1,*], **Marcos Blanco** [1], **Jorge Torres** [1], **Jorge Nájera** [1], **Álvaro Santiago** [1], **Miguel Santos-Herran** [1], **Dionisio Ramírez** [2] and **Marcos Lafoz** [1]

[1] Centro de Investigaciones Energéticas, Medioambientales y Tecnológicas (CIEMAT), Government of Spain, 28040 Madrid, Spain; marcos.blanco@ciemat.es (M.B.); jorgejesus.torres@ciemat.es (J.T.); jorge.najera@ciemat.es (J.N.); alvaro.santiago@ciemat.es (Á.S.); miguel.santos@ciemat.es (M.S.-H.); marcos.lafoz@ciemat.es (M.L.)

[2] Centro de Electrónica Industrial (CEI), Universidad Politécnica de Madrid, 28006 Madrid, Spain; dionisio.ramirez@upm.es

* Correspondence: gustavo.navarro@ciemat.es; Tel.: +34-91-335-71-99

Abstract: The aim of this paper is to present a methodology for dimensioning an energy storage system (ESS) to the generation data measured in an operating wave energy generation plant connected to the electric grid in the north of Spain. The selection criterion for the ESS is the compliance of the power injected into the grid with a specific active-power ramp-rate limit. Due to its electrical characteristics, supercapacitor (SC) technology is especially suitable for this application. The ESS dimensioning methodology is based on a mathematical model, which takes into account the power generation system, the chosen ramp-rate limit, the ESS efficiency maps and electrical characteristics. It allows one to evaluate the number of storage cabinets required to satisfy the needs described, considering a compromise between the number of units, which means cost, and the reliability of the storage system to ensure the grid codes compliance. Power and energy parameters for the ESS are obtained from the calculations and some tips regarding the most efficient operation of the SC cabinets, based on a stepped switching strategy, are also given. Finally, some conclusions about the technology selection will be updated after the detailed analysis accomplished.

Keywords: supercapacitor; energy storage; wave energy; dimensioning; efficiency; grid code; renewable energies

1. Introduction

The increased environmental awareness together with the fossil fuel availability reduction, have fostered the development and integration of renewable energy sources (RES) in the last decades [1]. In this sense, hydro, solar, and wind energy sources have been extensively researched and consolidated, whereas other RES as wave energy remain a few steps behind in terms of technology readiness level (TRL). Regarding wave energy, and given the significant potential enclosed in the waves [2], several wave energy farms have been deployed and tested, particularly in areas with high oceanic resource [3]. Thus, the numerous projects developed during the past years in Europe, United States, and Asia have pushed the wave energy technology to a precommercial state (TRL 7), and the first commercial projects are expected to be implemented in niche markets in the near future [2,4–6].

This paper focuses on wave energy converters (WECs) as the device selected for extracting the wave energy and converts it into electricity. For a thorough review of WECs and other wave energy devices, see [7].

The aforementioned integration and connection of wave energy farms, each one composed by a set of WECs, is not exempt of drawbacks. As with other non-dispatchable

RES (wind and solar energy), wave energy farms can have a considerable impact on the stability, quality, and reliability of the power grid [8,9]. Given the intermittent nature of the source, i.e., the waves, the power generated by a WEC also follows an intermittent profile with severe power fluctuations [10]. As a result, the power grid can suffer from sudden frequency deviations, and voltage distortion such as harmonics or flicker [9–11]. These frequency and voltage issues may cause the wave energy farm to not be compliant with the grid codes of the transmission system operators (TSOs) and, hence, make wave energy farms not suitable for being included in the electricity generation mix of a country [8]. In [12,13] an introduction about the study on grid compliance and standardization of renewable generation and other energy systems connected to the power grid is provided. In [13–17] the grid codes of different countries (European and non-European) and the corresponding projects about renewable power are compared and summarized. The impact of grid code regulations on stability is also analyzed. Additionally, these papers provide the information about the future trend of grid code requirements. The main requirements in most of grid codes include reactive power, frequency regulation, fault ride through, power quality, and communication.

Several solutions for solving this issue have been proposed in the literature, including advanced control strategies [18–20] and proper WECs location in the wave energy farm [21]. In [22] an active control for a tidal turbine is developed to grid code requirements in terms of active and reactive powers (P, Q) and, conversely, the voltage at the point of common coupling and reactive power (U, Q). However, the most promising solution for solving power quality issues, which encompass the vast majority of articles of this topic, is the utilization of an energy storage system (ESS) for a combined operation together with the wave energy farm. In this sense, the ESS will store energy when the power generated by the WECs overcomes a certain value, and it will deliver power when required by the control strategy [21].

Different energy storage technologies have been analyzed in the literature for being integrated with WECs, aiming for grid code compliance: battery energy storage system (BESS), flywheel energy storage system (FESS), and supercapacitor energy storage system (SCESS) or a hybrid energy storage system (HESS). All three technologies are able to provide a fast response in the range of 10–50 ms when the control strategy demands it [23,24].

BESSs have been studied in [25] for a combined operation of a wind turbine and a WEC, including a predictive control in order to not overcome the maximum power fluctuations allowed by the Irish grid code and the UK national grid code. The work published in [26] uses a BESS for smoothing the output power of a WEC, in order to have an acceptable power quality for a general grid code defined by the authors.

FESS have been studied together with a wave farm in [27] for controlling the power output of the complete installation, aiming for being compliant with the Nordic grid code. The authors in [27] develop a control based on three stages, achieving a reduction up to 85% in the power output peak. A control strategy is proposed for power smoothing in a hybrid wave energy plant. The control strategy is based on a power filtering process.

Grid code compliance with SCESS has been studied in [28,29], validating control strategies for compensating WEC power oscillations. A finite predictive control is applied to the study proposed in [28], where the SCESS is located in the DC link of the back-to-back power converter. The analysis performed in [30] include an experimental validation in a laboratory test bench of a control that includes a state of charge compensator for the SCESS. In [30] a SCESS is studied to smooth the power extracted from waves by a grid connected linear electric generator. A complete model of the system is developed in Simulink-MATLAB to test the system under varying system conditions (faults with and without the SCESS).

Another possibility is to use a hybrid energy system (HESS) consisting of two different storage technologies. For example, in [29] a power management system for a grid connected OWC wave energy converter with a HESS (battery/SC) is proposed. Performance of the

control system is evaluated in two case studies, fixed and variable operating speed. In [31] an optimization algorithm is aimed at splitting the power required between the battery and SCs of a HESS. This ESS is used to smooth the power oscillations for a wave energy conversion connected to the public grid. The proposed algorithm, among other things, considers minimizing the losses of the storage system and maximizing the battery lifetime.

Apart from those three ESSs, other authors decided not to select a specific ESS, but studied the application of a generic ESS together with a WEC. In this sense, authors in [32] combined a wave farm model with a small ESS for being compliant with the Irish, UK, and Nordic grid code. The study includes a modeling strategy for the wave-to-wire system of WEC arrays. Moreover, the work published in [33] studied the integration of a generic ESS for achieving the grid code requirements at the point of common coupling (PCC), using real location data. The authors also propose a real-time technique for the centralized control of the wave farm, which is validated in critical scenarios such as weak grids. In [34] an adaptive energy filter is proposed to smooth renewable power fluctuations in function of the input power level. The novelty of this paper resides in the robustness of the proposed filter against changes in the level of the generated power (fluctuating in the case of renewable sources). This method is generic and it can be applied to any ESS (BESS, FESS, SCESS, and SMES).

As it has been described above, the combined effects of using a WEC with different ESS has been analyzed, and the benefits for meeting the grid code requirements are clearly stated in the literature. However, from an industrial point of view, knowing that including ESSs is beneficial for integrating wave energy in the grid is as important as knowing the proper size of the ESS, in terms of power and energy. ESSs are expensive equipment, and under or oversizing can result in premature degradation and incompliancy with the grid codes, or unnecessary economic investment, respectively. Hence, ESS dimensioning studies for wave energy become of the utmost importance.

In this regard, the works published in [3,24] propose a dimensioning methodology for a generic ESS integrated with a WEC, without focusing on a specific technology, and based on efficiency and grid code compliancy in terms of frequency. Authors in [24] include a methodology validation for non-regular waves. A further validation with real data from Tenerife is performed in [3]. Moreover, authors in [35] proposed a SCESS dimensioning methodology, which includes an ageing model without temperature dependence, and with no particular focus on grid code compliancy.

For wave energy applications, SCESSs and FESSs perform better that other ESSs in terms of efficiency [36]. Although SCESSs and FESSs present similar characteristics in terms of TRL, power and energy range and number of cycles [23], SCESS is the ESS technology selected by the authors to perform the analysis of this work, since power and energy levels are appropriate, a better economic alternative has been found in terms of €/kW and the system fits better within the available space at the power plant.

A case study is proposed to illustrate the methodology, with the real profile of a wave power generation plant and a real SCESS. To reduce fluctuations in the power delivered to the power grid a specific active power ramp rate (%/min) is set. It is a characteristic parameter of the grid code standards. The proposed methodology allows the establishment of other types of limitations that conform to the existing grid codes in different countries.

The paper is structured as follows: in Section 2 the wave power generation plant on which this study is based is described, in Section 3 the SCESS cabinet on which the complete SCESS (technology, power loss calculation, and efficiency map) is based is described, in Section 4 the results obtained from a simulation model that integrates both the SCESS and the wave generation profile are presented and commented and, finally, in Section 5 some final conclusions are detailed.

2. Wave Power Generation Plant

The study of using supercapacitors (SCs) as a storage solution for systems that harvest energy from waves to comply with the grid code is based on the wave power generation

plant located in the breakwater at the harbor in Mutriku (Spain). The plant was inaugurated in 2011 and has been delivering power into the electric grid ever since. The technology used to extract energy from waves is called the oscillating water column (OWC) with a total installed power of 296 kW, comprising 16 equal turbines of 18.5 kW each [37]. The principle of these oscillating water column converters (OWC-WECs) is based on the pressure variation of the air contained in a chamber when the wave motion enters it. When the wave arrives, the contained air is expelled at high pressure through an orifice located at the upper part of the chamber. The air drives a turbine whose shaft is coupled to an electric generator. When the wave retreats, the water level in the chamber decreases. This causes the pressure inside the chamber to drop and the air to be sucked in through the upper hole. The turbine always rotates in the same direction regardless of the direction of air circulation, so that the rotation in the shaft is more or less continuous. The connection to the local distribution grid of the generation plant is made through a 460 V/13.2 kV power transformer. Figure 1a shows the electrical diagram of the wave power generation plant connected to the grid. Figure 1b shows an aerial image of the power plant.

(a) (b)
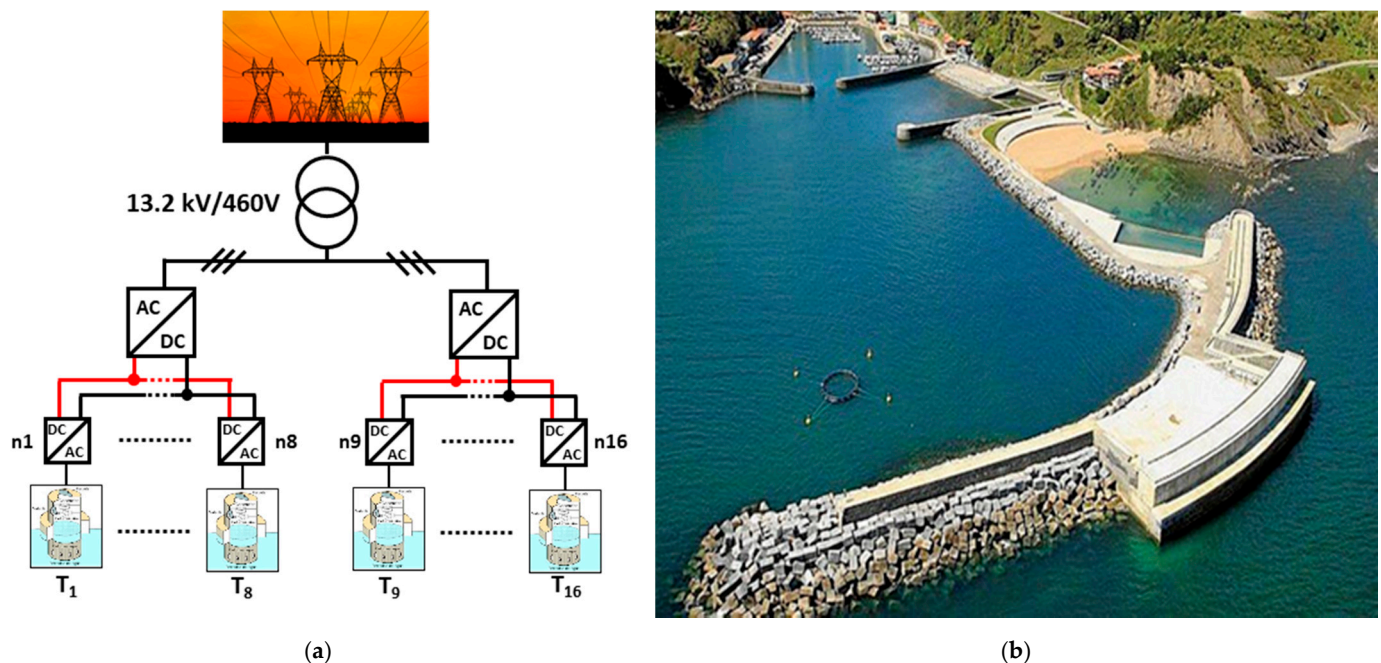
Figure 1. (**a**) Electrical diagram of the wave power generation plant and (**b**) aerial photo of the wave power generation plant integrated in the breakwater of Mutriku port.

3. Description of an Energy Storage System Based on SCs

Electric double layer capacitors (EDLCs) [30], commonly known as supercapacitors, are electrochemical capacitors composed of two conductive porous electrodes immersed in an electrolyte, between which a separator is placed. The electrodes are based on a sheet, usually made of aluminum, covered by activated carbon or carbon nanotubes. The electrolyte is the key element in determining internal resistance or equivalent series resistance (ESR). Nonaqueous solutions, such as acetonitrile or propylene carbonate, are often used because they support higher stress. The separator must allow the circulation of ions but avoid contact between the two electrodes. SCs, like conventional capacitors, store charge electrostatically and there is no charge transfer between the electrode and the electrolyte. EDLCs use double electrochemical layers to store energy. When a voltage is applied between the electrodes, the charge accumulates on the surface of the electrodes. Following the natural repulsion of oppositely charged, ions in the electrolyte solution spread through the separator into the pores of the oppositely charged electrode. These

double layers, together with an increase in surface area and a reduction in the distance between electrodes, allow SCs to achieve energy densities much higher than those of conventional capacitors [38]. Since there is no charge transfer between the electrolyte and electrode there are no changes in the chemical composition. For this reason, the storage of charge in EDLCs is reversible and is not associated with a significant loss of capacity with the number of charge and discharge cycles, which is not the case in electrochemical batteries.

SCs are especially suitable devices for high power applications with a relatively low energy capacity compared to batteries [39,40]. It has a lower cost than batteries in terms of power, a complete cycle efficiency of around 95%, the possibility of a high number of charge-discharge cycles (up to a million as per the datasheets) and a useful life of 20–25 years. The operating temperature range is between −40 and 60 °C, much wider than that of batteries, without significant impact on their response. The energy that a capacitor of any type is capable of storing is dependent on its capacitance and its voltage. The capacitance (C) is a constructive parameter related to the electrical charge that the device is capable of storing and that depends on constructive aspects such as the permeability of the dielectric, the area of the metallic plates and the distance between them. On the other hand, the maximum voltage between terminals depends on the insulation conditions of the dielectric that is between the two electrodes that make up the SC.

Regarding capacitance, it should be taken into account that EDLCs are not linear capacitors, but that the capacity depends on the voltage, as shown in Figure 2 [41,42]. In the case of cells, manufacturers provide values for capacitance and ESR. The capacitance value is only a mean value in the voltage operating range. For the basic cell upon which this study was based (BCAP3000 commercialized by Maxwell in the past) the maximum capacity value at the beginning of the operational life was above 3000 F, being 3000 F was the mean value. To model this evolution of the capacitance, an experimental loading process was performed in which measured capacitance was calculated in small voltage increments. Figure 2a shows the evolution of capacitance with voltage. It presents a quadratic relationship with the voltage as indicated in the following equation:

$$C(V) = -95.756 \cdot V^2 + 613.58 \cdot V + 2216.6 \qquad (1)$$

V: Voltage measured in the terminals of the SC (V);
C (V): Capacitance as a function of the voltage (F).
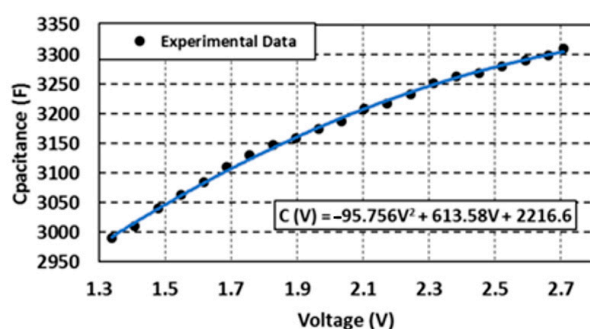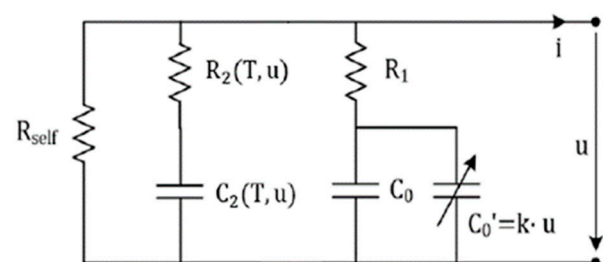
(a)   (b)

Figure 2. (**a**) Evolution of the capacitance value as a function of the voltage in the BCAP3000 cell and (**b**) schematic of the electrical circuit used to model the behavior (voltage) of the supercapacitors (SCs).

An appropriate dimensioning of any storage system must take into account the power losses. The fundamental losses in the SCs are produced in the separator, in the positive and negative current collectors and in the positive and negative porous electrodes [40]. The total resistance of each of these parts is included in the ESR. It must be taken into account that the ESR value is not constant, but depends on the voltage in the cell, the temperature

and the frequency of the current that passes through the cell. To model the losses in the SCs, which will be explained later, an electrical circuit like the one shown in Figure 2b is used [41].

Another difference between batteries and SCs is that, while in batteries the voltage is relatively constant regardless of the state of charge (SoC), in SCs the voltage is more or less linear with the SoC. For this reason, the integration of this type of ESS into industrial applications is usually done through DC/DC power converters. This characteristic means that the SCs cannot be fully discharged, since working at too low of a voltage would greatly penalize the performance of the power converter. For this reason, it is common to define a discharge limit up to half their maximum voltage, which means using $\frac{3}{4}$ parts of their theoretical energy, as can be seen in Equation (2).

$$E_{availablel} = \frac{1}{2} \cdot C \cdot \left(U_{MAX}^2 - U_{MIN}^2 \right) = \frac{1}{2} \cdot C \cdot \left(U_{MAX}^2 - \left(\frac{U_{MAX}}{2} \right)^2 \right) = \frac{1}{2} \cdot C \cdot U_{MAX}^2 \cdot \frac{3}{4} \quad (2)$$

U_{MAX}: Maximum operating voltage measured on the SC (V);
U_{MIN}: Minimum operating voltage measured on the SC (V);
C: Average value of SC capacitance (F).

3.1. Description of the Real SCESS Module on Which this Study Is Based

The unit module of SCs is made up of 8 drawers connected in series as shown in Figure 3. Each of the drawers has, in turn, 30 units of BCAP3000 cells connected in series. The main electrical characteristics of each cell are a nominal voltage of 2.7 V, capacity of 3000 F, and energy of 3 Wh. Therefore, the nominal capacity of the cabinet was 11.7 F and the total energy available was 500 Wh. If each cell is discharged to half its voltage, the total energy available is $\frac{1}{4}$ of the total energy. Despite this fact, and as mentioned in the previous point, the minimum working voltage of each cell was set at half the nominal voltage so that the performance of the DC/DC converter that connects the SCESS with the DC bus does not decrease considerably. Therefore, the theoretical operating voltage range of the cabinet was approximately 381-636 V. The cabinet was provided with 16 electronic boards to measure the voltage evolution of each cell. Another 30 temperature measurement channels were also used to monitor the maximum temperature of the cells and check it did not exceed 65 °C. Analog measurements of voltage and temperature were monitored due to a Concerto F28M35H52C microcontroller commercialized by Texas Instruments (12500 TI Blvd., Dallas, Texas 75243 USA) that was placed inside the same cabinet. This microcontroller acted as a web server to access the temperature and voltage measurements via the internet.

The cabinet had a cooling extractor turbine located in its upper part. The rotation speed of this turbine varied depending on the temperature in the cells. Additionally, each of the cells has a hardware protection system so that the cells did not exceed their maximum voltage. In addition, this system allows the total voltage to be balanced so that it is distributed equally among all the cells. Figure 3a shows the state of the cabinet during a balancing process.

3.2. Operation Limits and Calculation of Power Losses and Performance of the SCESS

As mentioned above, in order to decide which storage system is best suited to a certain application, it is very important to consider its energy efficiency. In general, storage systems are complex non-linear systems and it is not easy to know their performance over the entire operating range. One of the parameters on which efficiency depends is the state of charge (SoC), that is, the operating point at which the system is working. In the case of SCs, efficiency is a function of current and voltage (SoC = f (V)) at each moment. In the present application the ESS, formed by supercapacitors, is connected to a DC bus through a DC/DC converter. Therefore, to calculate the overall efficiency it is necessary to also take into account the performance of this converter. Another parameter on which

the efficiency of the ESS depends is the duty cycle. It is necessary to take into account the frequency with which the SCs are charged/discharged, because, among other parameters (temperature), the value of the series resistance (ESR) depends on this frequency. Therefore, when a performance value is provided, the associated duty cycle must be specified. In the sizing of the storage system for the present application, the overall performance of the set composed by the electronic converter and the SCs for each operating point has been considered. The process followed to calculate these losses is explained in the next points.

(**a**)   (**b**)
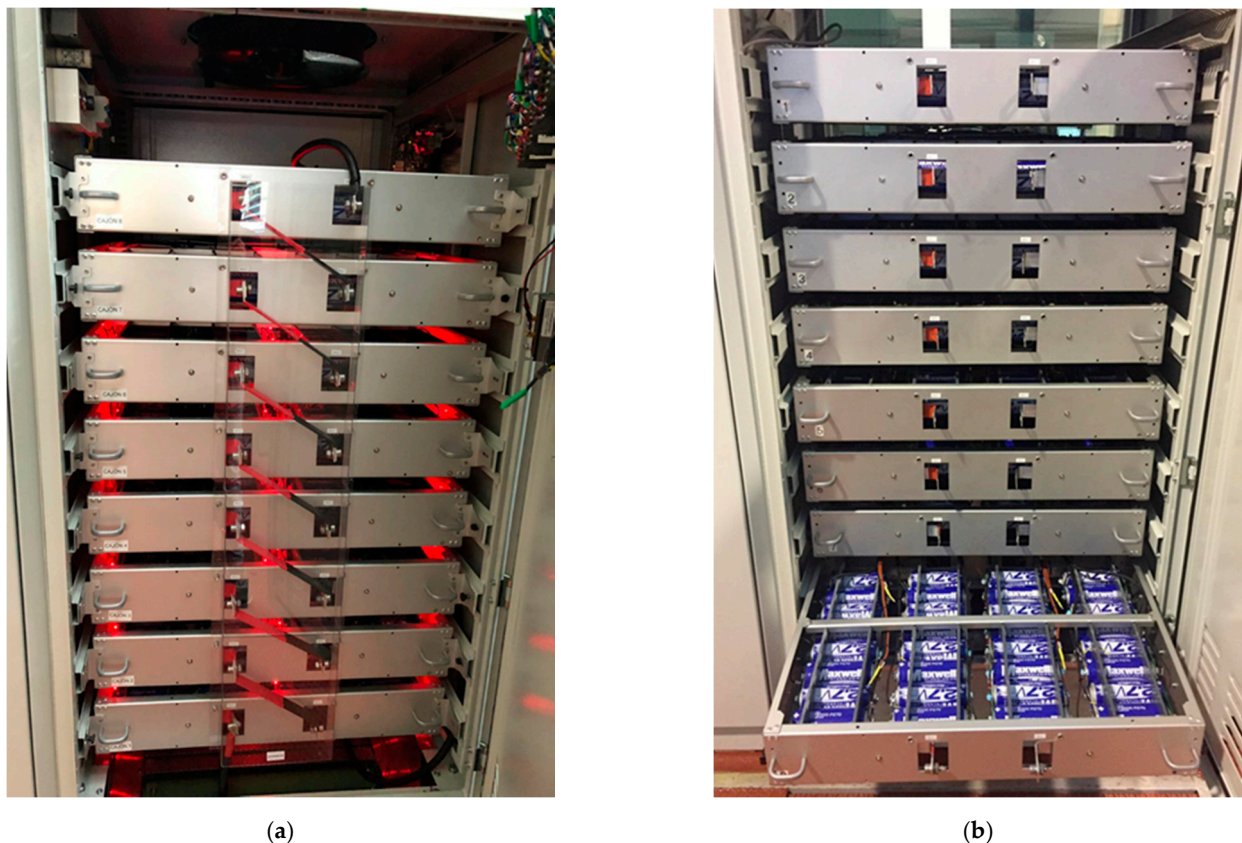
Figure 3. (**a**) Image of one supercapacitor energy storage system (SCESS) module during a voltage balancing process between cells and (**b**) image of one of the eight drawers that make up the SCs cabinet upon which this study is based.

As has already been commented, the SCESS is connected to a DC bus through a power converter. Another converter, connected between the electrical grid and the DC bus, keeps the voltage value of this bus at 950 V. This DC/DC converter regulates the charge/discharge current according to the received power command. The maximum power and energy available for each SC cabinet (unit module) is 125 kW and 0.5 kWh respectively. These values correspond to the following operating limits for each cell that makes up the SC cabinet:

- $U_{SUPERCAP\_max}$: 2.65 V;
- $U_{SUPERCAP\_max}$: $0.6 \cdot U_{MAX}$;
- $I_{SUPERCAP\_max}$: 200 A.

The nominal voltage of each cell was 2.7 V (absolute maximum voltage is 2.85 V), but the maximum operating value was set at 2.65 V for two reasons. The higher the voltage in the SCs, the more accelerated their ageing. Reducing the maximum voltage by 0.05 V greatly lengthened the lifetime of the SCs. On the other hand, the ESS was formed by a series connection of cells and the distribution of the total voltage between all of them was not perfect. To ensure that the voltage in any cell was higher than 2.7 V, 2.65 V was set as the maximum value. The total working voltage range of each cabinet will be 382-636 V.

These limits imply an input and output voltage ratio in the DC/DC converter of 1/3-2/3, which did not significantly restrain its performance [43].

3.2.1. Power Losses in the Equivalent Series Resistance (ESR)

In order to calculate the performance of the storage system, in addition to taking into account the efficiency of the storage system (ESR losses) and the converter, the losses in the connection plates, in the cables and in the voltage balancing system were calculated [36]. In this case, the variation of the ESR and capacitance with the temperature in the cell was not considered, since each cabinet had a cooling turbine in the upper part that maintains the temperature of the cells in the working range of 25-40 °C. In this temperature range the variation of both parameters (ESR and C) was very small. Regarding the variation of capacitance with frequency, it was not studied in this paper, only analyzing the variation with voltage.

To calculate the power losses in the ESR, Equation (3) must be taken into account:

$$P_{ESR}(t) = U_{SC}(t) \cdot i_{SC}(t) \tag{3}$$

$P_{ESR}(t)$: Instantaneous power losses;
$U_{SC}(t)$: SC voltage;
$i_{SC}(t)$: Instantaneous current through the SCs.

If the current is considered as a periodic function of period T, it can be written as a Fourier series:

$$i_{SC}(t) = \sum_{i=0}^{+\infty} I_{SC}(i) \cdot \sin(iwt + \vartheta_i) \tag{4}$$

$I_{SC}(i)$: Harmonic component of the current;
w: Angular frequency.

The voltage across the ESR can be expressed as:

$$U_{ESR}(t) = \sum_{i=0}^{+\infty} ESR(iw) \cdot I_{SC}(i) \cdot \sin(iwt + \vartheta_i) \tag{5}$$

$U_{ESR}(i)$: Voltage across ESR
$ESR(iw)$: ESR value for each frequency

If Equations (4) and (5) are multiplied, the expression for the instantaneous power losses in the ESR is obtained. Applying the Lagrange identity and the orthogonal property of sine and cosine the total power losses can be expressed as [40]:

$$P_{ESR}(t) = I_{RMS}^2 \cdot \left[\sum_{i=0}^{+\infty} ESR(iw) \cdot \frac{I_{SC(i)}^2}{I_{rms}^2} \right] = I_{RMS}^2 \cdot ESR(eq) \tag{6}$$

I_{RMS}: r.m.s value of the current;
$ESR(eq)$: Total ESR.

To calculate the equivalent resistance in series for each frequency, it is necessary to complete an analysis of the SCs in the frequency domain. This analysis is based on experimental tests and on the design of a simulation model whose frequency response is adjusted to the results obtained experimentally. A complete analysis of the frequency response of the cell model (BCAP3000) on which the present study is based is presented in [44]. In this way, using Equation (6) the efficiency (η_{ESR}) of the SCESS cabinet can be calculated including the losses in the ESR for a given duty cycle (frequency) as per:

$$\eta_{ESR} = \frac{U_{SC} \cdot I_{rms}}{U_{SC} \cdot I_{rms} + P_{ESR}} \tag{7}$$

U_{SC}: SC voltage;

I_{rms}: r.m.s value of the current through the SC.

Figure 4a,b shows the evolution of the power losses in the ESR and the efficiency of the ESS as a function of the current flowing through the SCs and the voltage measured at the terminals. As expected, the higher the current through the capacitors, the higher the power losses in the ESR.

(a)

(b)
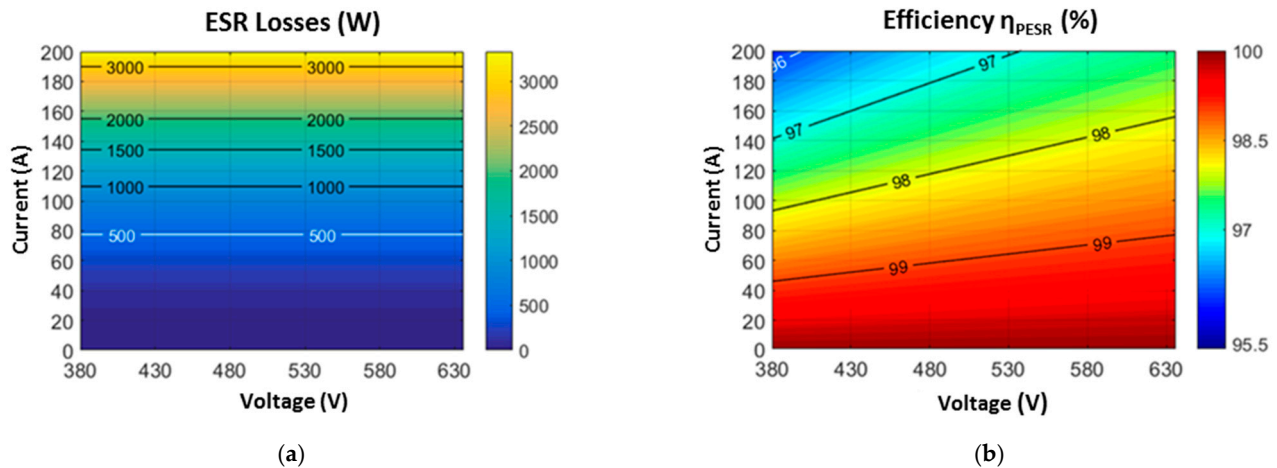
Figure 4. (**a**) Power losses in the equivalent series resistance (ESR) as a function of the current and voltage measured in the SC cabinet and (**b**) efficiency map of the module due to ESR losses.

3.2.2. Voltage Balancing System Power Losses

As mentioned above, the ESS was made up of a series connection of cells, whose maximum voltage was 2.65 V, in order to achieve voltage levels more typical of industrial applications. Due to manufacturing tolerances, not every cell has the same capacitance or ESR, which means that the distribution of the total voltage between the different cells is not exactly the same. Therefore, there is a voltage supervisor hardware that prevents any cell from exceeding the voltage limit value (2.7 V) and facilitates the equitable distribution of voltage [45–47]. This system is based on the dissipation of the power in a resistance when the voltage in any of the cells exceeds a predetermined threshold value (approximately 2.6 V). Below this value the protection system does not work. The current and resistance where that current is dissipated is known, so the power losses can be derived from voltage measured in the SCs as follows:

$$P_{V\_Balancing} = R_{DIS} \cdot I^2_{DIS}(U) \tag{8}$$

$P_{V\_Balancing}$: Voltage balancing system power losses;

R_{DIS}: Power dissipation resistance;

$I^2_{DIS}(U)$: Current dissipation as a function of the measured voltage.

Figure 5 shows the power losses map of the voltage balancing system as a function of the current flowing through the ESS and its voltage. Compared to the power losses calculated in the ESR, these losses can be considered negligible.

3.2.3. Cooling System and Electrical Connection Plates Power Losses

Each SCs cabinet has an extractor cooling turbine on top because a natural cooling system is not sufficient for these power requirements. It is a variable speed turbine whose control depends on the temperature measured in the SC cells. The higher the temperature in the cells, the higher the rotation speed. The objective of this refrigeration system is to keep the temperature of the SCs below 40 °C. It is known that SCs age faster the higher the stress to which they are subjected and the higher their temperature [45]. Ageing in this

ESS type causes a decrease in C and an increase in ESR. This results in a loss of available energy in the ESS with respect to its initial value and a loss of efficiency. On the other hand, uneven aging between cells causes an imbalance in the distribution of the total voltage and a limitation in the use of available useful energy. To calculate the losses at the refrigeration system, an equivalent electrical circuit has been implemented using MATLAB-Simulink [48] that models the refrigeration flow. Additionally, a turbine regulation curve has been established to improve its efficiency. Figure 6a shows the map of cooling system losses as a function of current and voltage between terminals. It can be seen that the higher the current, the higher the losses in the cooling system and in the connection bars. As in the previous case, the losses are low compared to the losses in the ESR.

(a)

(b)
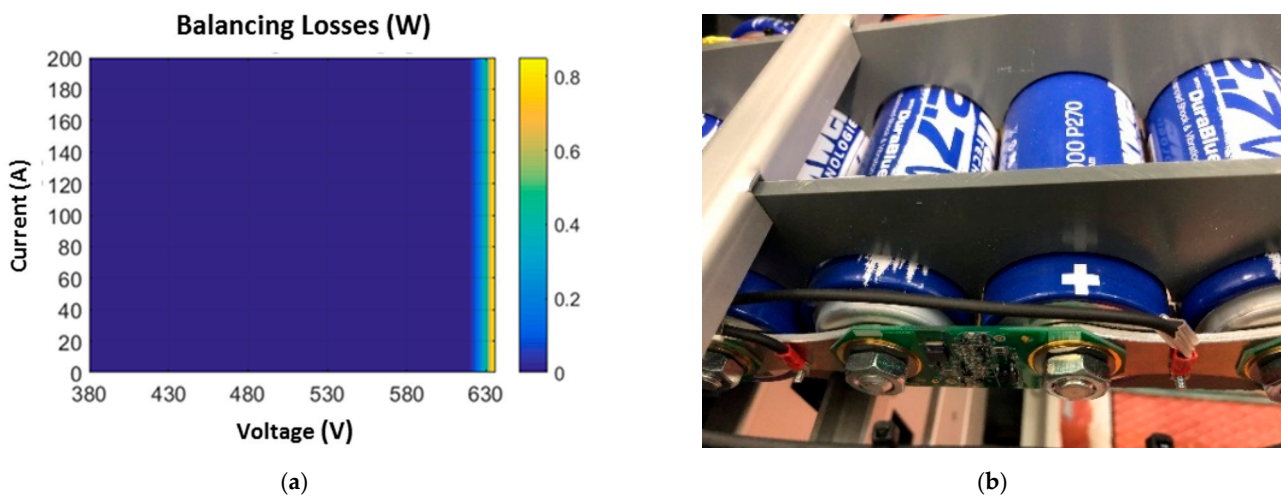
Figure 5. (**a**) Power loss map in the voltage balancing system as a function of current and voltage and (**b**) detail of the connection plates between the cells and of the voltage balancing system.

(a)

(b)
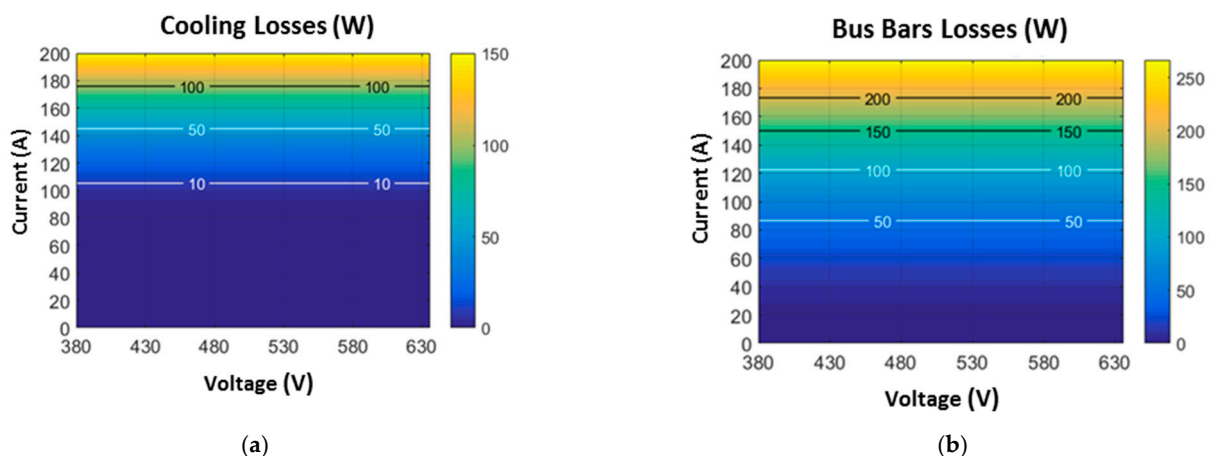
Figure 6. (**a**) Power losses map of the cooling system as a function of voltage and current and (**b**) power losses map in the connection bars between cells as a function of current and voltage.

Regarding the losses in the connection plates between cells [49], it must be said that they have a certain resistance and consequently a power loss depending on the current flowing through them. These are 3 mm thick aluminum plates supplied by the manufacturer. The resistance value of each connection plate is given by:

$$R_{CONNEC\_PLATES} = \frac{\rho \cdot l}{S} \tag{9}$$

R_{CONNEC_PLATE}: Resistance of connection bars;
ρ: Aluminum resistivity;
l: Connection plate length;
S: Connection plate section.

Therefore, the power losses in the plates (P_{CONNEC_PLATES}) are calculated as:

$$P_{CONNEC\_PLATES} = I^2_{SUPERCAP} \cdot R_{CONNEC\_PLATES} \cdot No_{SUPERCAP} \tag{10}$$

$I^2_{SUPERCAP}$: Current through the SCs;
$N_{SUPERCAP}$: Number of SCs connected in series.

3.2.4. Power Converter and Total Losses

Each SC cabinet was connected to a DC bus regulated at a voltage of 950 V through a DC/DC converter that regulated the charge/discharge current of the ESS. This current command was the consequence of the reference power value to supply/consume assigned to the SCESS. The generation of this power command and the control of the complete system will be explained in the next point. A 3-branch interleaved DC/DC converter was used to exchange power between the ESS and the mentioned DC bus. This converter was bidirectional in the current to allow both charging and discharging of ESS. Figure 7 shows the topology and the input and output voltage levels of the converter [50,51].

The DC/DC power converter is a voltage source converter that regulates the charge/discharge current of the ESS. The control strategy was designed to operate in the discontinuous driving mode to improve its efficiency. The total current that passes through the SCs was distributed among the three output branches of the converter. The converter was modeled in MATLAB-Simulink to size the power components (filters, semiconductors, cooling system, etc.) and to verify the operation of the converter with the designed control strategy. On the other hand, the model implemented in MATLAB-Simulink allowed calculating the converter losses to obtain, as in the previous cases, the power converter losses as a function of the voltage and current through the SCs. The performance of the converter was calculated according to Equation (11):

$$\eta_{power\_converter} = \frac{U_{SC} \cdot I}{U_{SC} \cdot I + P_{converter\_losses}} \tag{11}$$

U_{SC}: Voltage of the SCs system;
I: Current through the SCs;
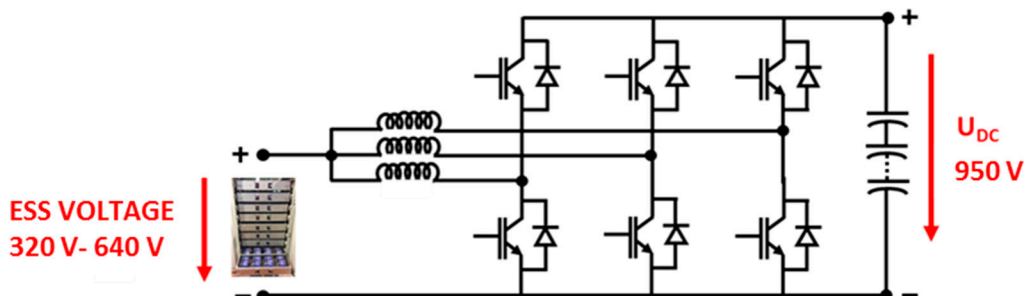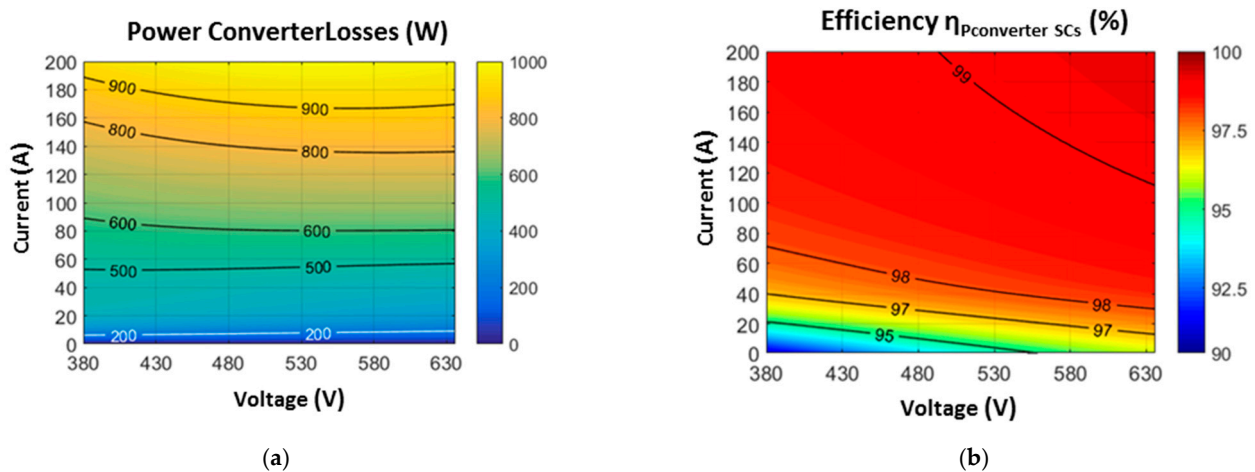$P_{converter\_losses}$: Power converter losses.

Figure 7. Electrical diagram with the voltage levels at the input and output of the DC/DC converter used.

Figure 8a shows the power converter losses as a function of the voltage and current through the SCs. Figure 8b shows the total efficiency of the power converter. The total losses of the power converter were higher with higher currents. However, the relative efficiency of the converter (with respect to the total power) was higher the higher the current through the SCs.

Figure 9a shows the total power losses of the SC cabinet as a sum of the previously calculated map (ESR, balancing and cooling system, bus bars, and power converter losses). Likewise, Figure 9b shows the total efficiency map of each cabinet as a function of the current and voltage.

(a)

(b)

Figure 8. (**a**) Power losses map in the DC/DC converter as a function of the current and voltage in the SCESS module and (**b**) efficiency map in the DC/DC converter as a function of the current and voltage in the SCESS module.

(a)

(b)
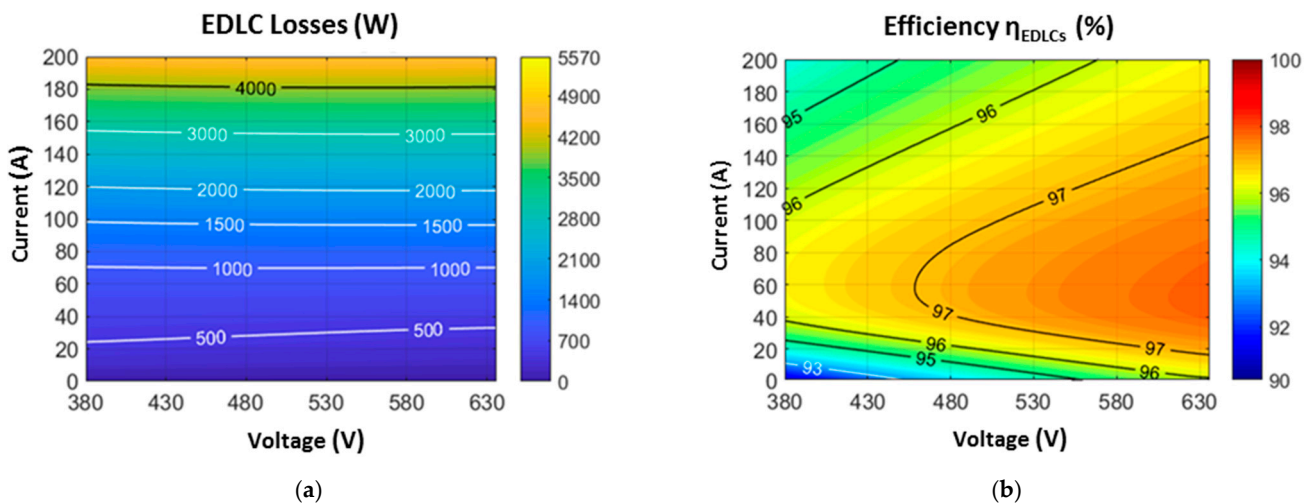
Figure 9. (**a**) Total losses map in the energy storage system (ESS) (sum of all commented power losses) as a function of current and voltage and (**b**) total efficiency map of the SC cabinet as a function of current and voltage.

4. Description and Results Obtained from the Simulation Model Developed

This section analyzed the case study chosen for the sizing of a SCESS that allows the power injected into the grid by a wave power generation plant to comply with the grid code standards. The generation profile studied is that of the Mutriku port plant located in Biscay (Spain) and managed by Biscay Marine Energy Platform (BIMEP) [52]. The representative study period is slightly longer than 1 month, from 7 May to 19 June 2020. The sampling time of the power measured during this period was 1 s. Figure 10 shows the wave power generation profile generated by 3 of the 16 water column converters during said period (in blue). The total power generated by the plant (in red) is also displayed (N.B.: criterion: negative sign is generated power). It can be seen how the power generated by the OWCs is highly variable due to the oscillating nature of the wave resource itself [53]. The generation

peaks can reach values of up to 10 times the mean value. Just as a curiosity, the maximum power peak in the generation period occurred on June 11, with a value of 163 kW.
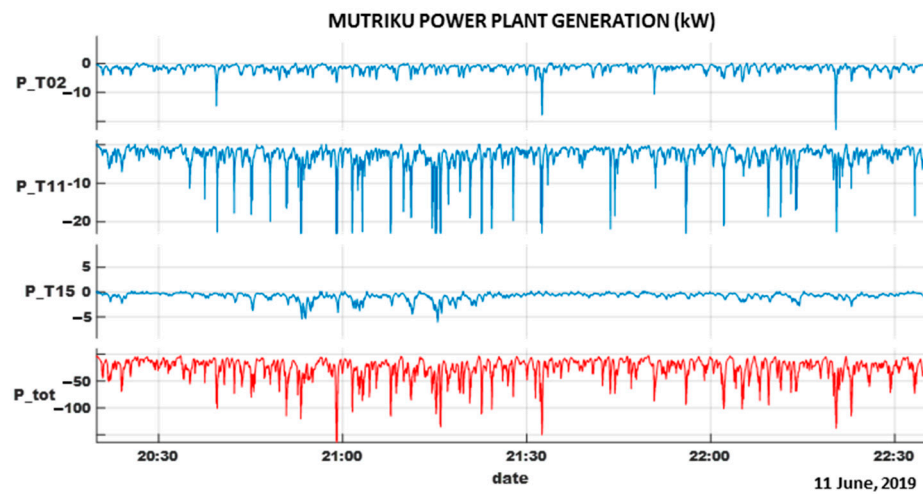

Figure 10. Power profile of three representative turbines of the wave power generation plant and total power in a stretch of time of the period studied.

4.1. Scheme of the Model Elaborated in SIMULINK-MATLAB and Its Input Parameters

For this study, a model has been developed using MATLAB-Simulink that includes the power generation data from the wave power plant for just over a month, the storage system based on several units of a real SC cabinet and the profile of the power that is exchanged with the electrical grid to comply with the different grid codes [54]. The ESS reference power profile is the result of subtracting the power from the generation plant and the target power profile to be injected into the grid [55,56]. The ESS, in addition to the SC cabinets, also integrates the DC/DC power converter. The scheme of the Simulink model is shown in Figure 11.
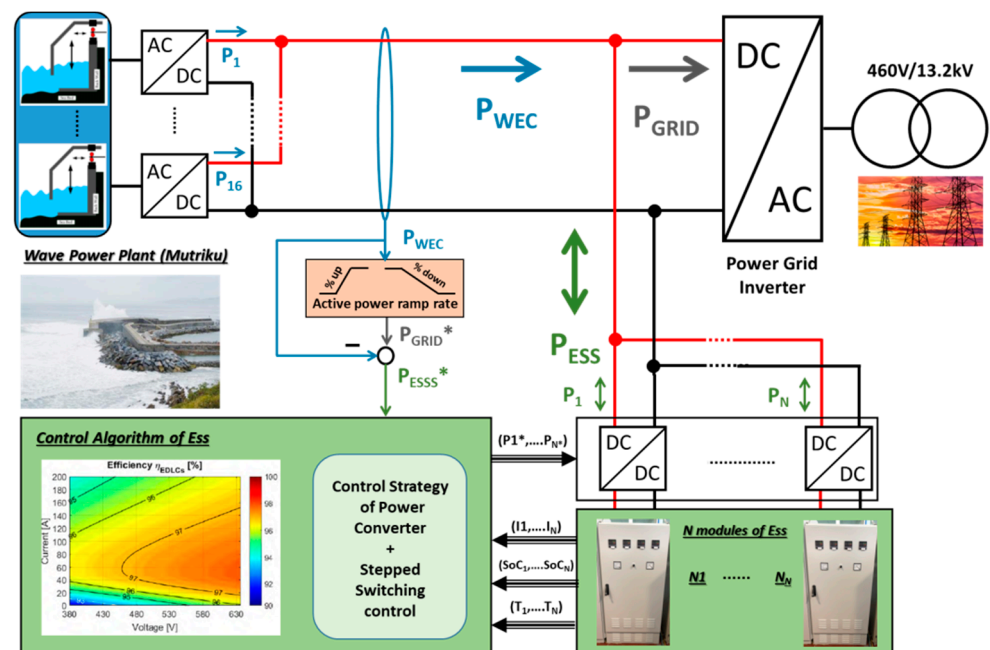

Figure 11. Simplified scheme of the model and control implemented in MATLAB-Simulink.

In order to be able to analyze all the available generation data, the full sample is divided into 15 min sections. It is set as a reference that the energy balance of the complete

storage system (ΔEESS) at the end of the complete generation period is zero. This means that the SoC of the storage system at the end of the analysis is the same as the initial one. In addition to the wave generation power profile, the other input parameters that the model has are: the maximum percentage of the rise ramp of the wave generation profile (% ramp-up/min) that can be injected into the grid, the ESS efficiency maps discussed in the previous section and the electrical parameters of each SC cabinet (maximum power, maximum and minimum voltage, available energy, and initial state of charge). From the limit value of % ramp-up, the value of the maximum percentage of the ramp down of the generation profile that can be injected into the grid was calculated so that the ΔEESS at the end of the generation period is null. In other words, for each allowed value of % ramp-up [57] there will be a value of ramp-down (%/min) that fulfills the previous condition (ΔEESS = 0). On the other hand, the model integrates the instantaneous SoC of each cabinet (voltage/current) to calculate the efficiency and the real instantaneous power that each SCESS module is capable of supplying/storing. Table 1 summarizes the main input parameters of the simulation model:

Table 1. Main input parameters of the simulation model.

Parameter	Meaning	Value
% ramp-up	Maximum ramp-up (%/min)	10
U_{MAX}	Maximum voltage per cell in the SC cabinets	2.65 V
U_{MIN}	Minimum voltage per cell in the SC cabinets	1.59 V
$SoC_{\_INITIAL}$	Initial State of charge of the SC cabinets	60%
$Energy_{\_USABLE}$	Usable energy respect to the total energy of each SC cabinet	0.5 kWh
P_{ESS_MAX}	Maximum Power provided by one SCESS module	125 kW

4.2. Results Obtained in the Simulation Model

Starting from ramp-up value (%/min) of 10, the value of % ramp-down that fulfilled that at the end of the complete generation period studied the ΔEESS = 0 was 7.22%/min. The ESS energy balance was calculated from the ESS power profile throughout the generation period. The power profile of the ESS was the result of subtracting the wave generation power profile and that same generation profile limited by the maximum ramp-up (%/min) and ramp-down (%/min) allowed (target power injected to the power grid). Figure 12 shows the generation profile throughout the entire period (in blue) and the target power profile that was injected into the grid after applying the aforementioned restrictions.
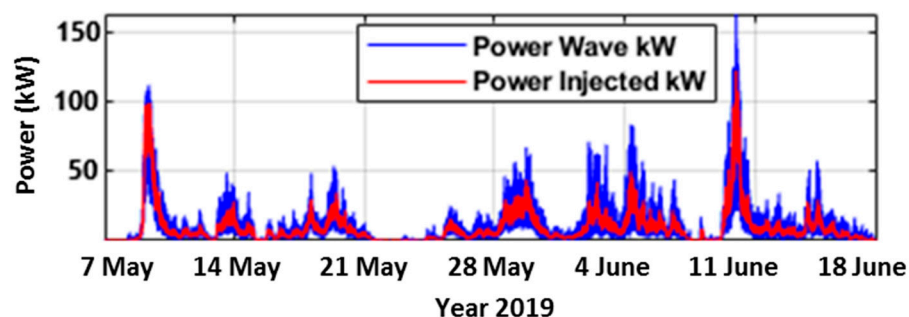
Figure 12. Profile of the generation of the plant (in blue) and theoretical objective profile to be delivered to the grid after applying the power ramp-rate limit.

To evaluate the actual energy required for the storage system, the efficiency maps calculated and introduced in the previous point were integrated, which incorporated the losses in the elements that exist between the SCs and the connection point with the

generation plant. Figure 13a,b shows the target power and energy profiles respectively of the ESS throughout the generation period to comply with the established grid codes. The maximum power requested from the storage system at the connection point was 111 kW (11 June).

(a)

(b)
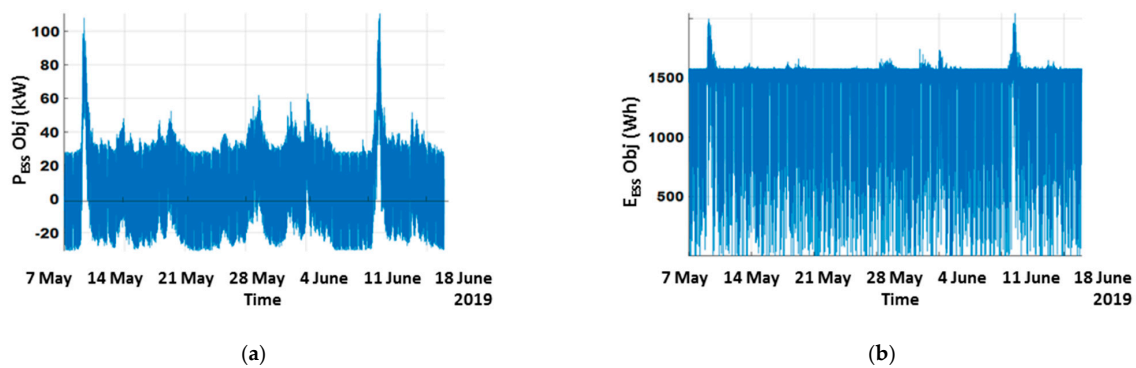
Figure 13. (**a**) Power profile that the ESS has to supply to meet the active power ramp-rate limit requirement and (**b**) ESS energy calculated in 15 min periods from required power.

Once the energy and power required from the ESS are known, the optimum number of SC cabinets must be calculated to reduce the oscillations of the power delivered to the grid. To do this, the joint cumulative distribution function of the power and energy required from the ESS was calculated in 15 min steps throughout the entire generation period. This function gives an idea of the percentage of time when the restrictions applied to the power delivered to the grid can be met. Figure 14a shows the values of the normalized cumulative probability of the ESS with respect to power and energy calculated in 15 min steps. Most of the values were found at power figures above 20 kW and energy figures greater than 1400 Wh. On the other hand, areas in Figure 14b represent the areas relative to the percentage of time that the power and energy needs are met as a function of the number of SC cabinets chosen. Considering that each cabinet has a maximum power of 125 kW and an energy of 500 Wh, the resulting black line is shown in black in Figure 14b. If three cabinets are chosen, the percentage of time that the generation curve would be smoothed, complying with the grid codes would be almost 80%. However, if four cabinets were selected, the objective would be met 100% of the generation time on which the study was made. The decision to install three or four cabinets will depend on a further analysis of the particular consequences of the power oscillations in terms of frequency excursions. It can be observed in any case that the ESS would be oversized in terms of required power for the present application while fulfilling the energy requirements, more restricting in this case In other words, the maximum current that each cabinet is capable of giving could be limited to a value lower than the set limit of 200 A, seeking a more optimal ESS point of efficiency complying with the established restrictions for the same percentage of the time.

Considering that 3 o 4 SC cabinets would be required, the most efficient operation would lead to switching between the SC cabinets according to the power and energy needs, the strategy known as "stepped switching". In this mode, a minimum power value is set, which takes into account the SoC, below which the corresponding SC cabinet is disconnected and another one with a higher SoC takes over and starts up. The maximum power that each cabinet is capable of giving is a function of the SoC and the operating point where it is located (in the efficiency map). What is sought with this strategy is that the efficiency of the cabinets in operation is always above a certain threshold, applying the efficiency maps and knowing the voltage and current that each cabinet is supplying. Another possibility would have been the simultaneous operation of all the chosen cabinets. That is, each cabinet would give the same power and would be working at the same load regime all the time. The total power required would be equally shared among them. However, this strategy known as "all-in, all-out" reduces the efficiency of the ESS as a

whole compared to the efficiency achieved with the previous strategy [58–60]. Figure 15 shows the real power profile delivered to the grid for a 10% ramp-up, a 7.22% ramp-down and an ESS made up of 4 modules of SCs.
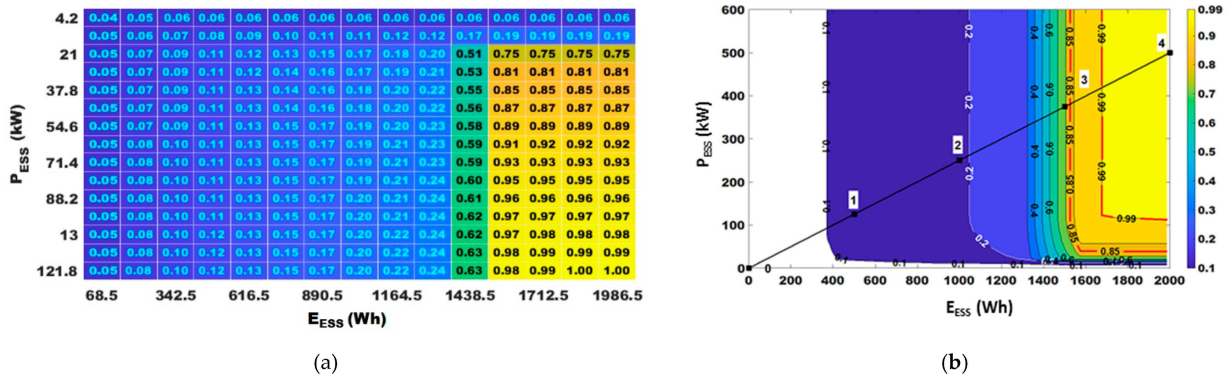

(a)

(b)

Figure 14. (**a**) Cumulative power and energy distribution function in the ESS and (**b**) cumulated distribution function for selection of the number of cabinets necessary to cover a certain number of cases of the proposed objective.
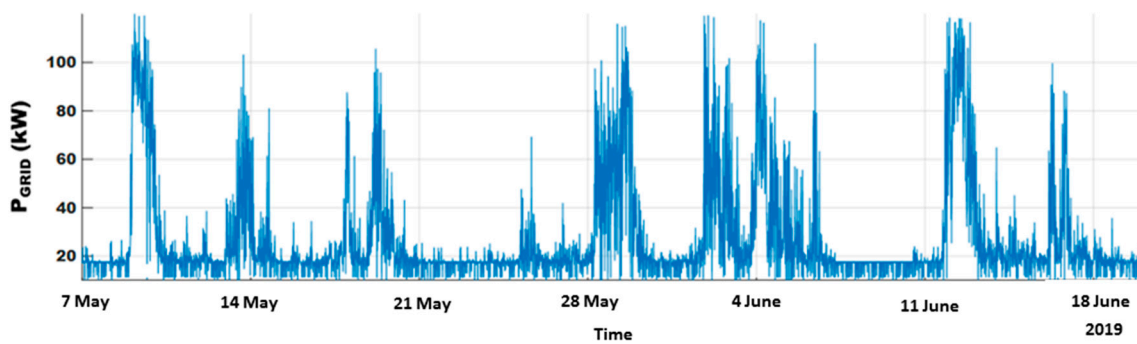

Figure 15. Power profile delivered to the grid throughout the generation period.

Figure 16a shows the percentage of time with respect to the complete generation period that each cabinet would work if 4 units were selected. On the other hand, Figure 16b shows a sensitivity analysis of the mean value of the reference power to be injected into the grid based on different grid codes (% ramp-up). Values from 10% to 23% (p.u./s) were taken. These values will correspond to respective ramp-down values, always complying that at the end of the generation period the energy balance in the ESS was zero. From the box-and-whisker plot it can be extracted that the median (Q2) was very similar in all cases as expected, around 20 kW. On the other hand, the atypical values of power delivered to the grid were below 5 kW and above 40 kW.

(**a**)

(**b**)
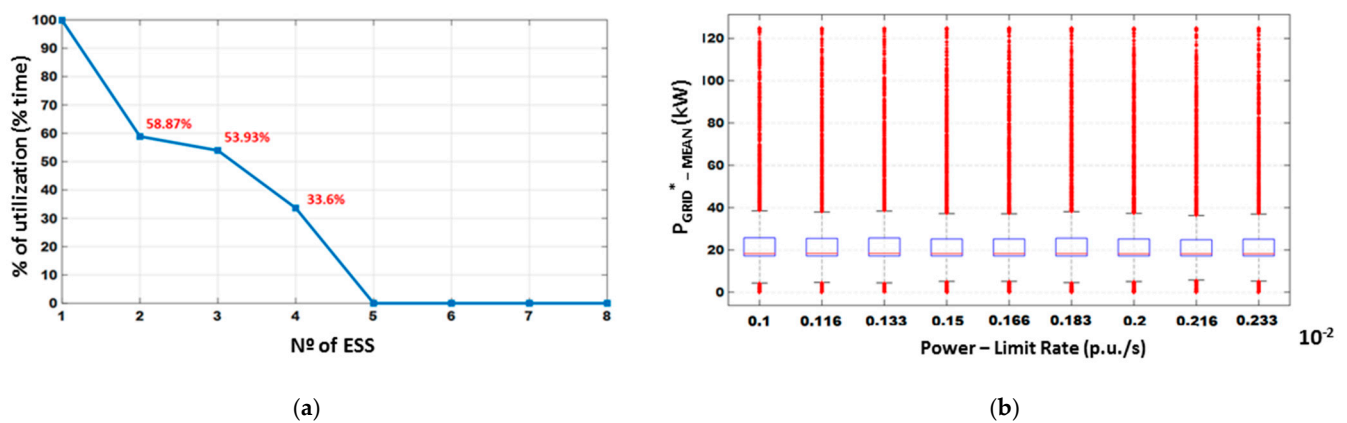
Figure 16. (**a**) Percentage of use of each of the four SC cabinets during the entire period studied and (**b**) box and whisker plot showing the average reference power values that will be delivered to the grid based on different active power ramp rate limits per minute (p.u./s).

5. Conclusions

This paper presents the methodology followed in the sizing of a SCESS in order to reduce the power oscillations of a real wave power generation plant connected to the electricity grid. The criterion followed to reduce the oscillations of the power injected into the grid is to limit the ramp-up of the power delivered by 10%/min and the ramp-down by 7.22%/min with respect to the generation profile. This criterion is based on the application of a grid code, which defines the requirements that a facility connected to a public power grid has to meet to ensure a safe, secure, and economic proper functioning. In this case, among all the parameters limited by the grid code standards, the active power ramp rate limit specified by regional transmission system operator (TSO) of each country is studied. For the sizing of the ESS, the calculated efficiency maps calculated of a real SC cabinet (on which this study is based) were drawn up to analyze the real power that the SCESS has to supply based on the measured current and voltage. Unlike other ESSs, such as batteries, the voltage in the SC is more variable and must be properly considered in order to try to operate, as far as possible, at the most optimal point of efficiency when there are several storage modules (cabinets) working in parallel. For the study shown, a model was developed in MATLAB-Simulink that integrated *n* modules of one ESS (SC + power converter), the wave generation profile and the power profile to be delivered to the grid.

Additionally, to select the ESS units that were necessary in this application, the cumulative probability of the ESS power and energy values (calculated in 15 min periods) that satisfy the established criteria were studied. For the dimensioning of any ESS it is necessary to find a compromise between the percentage of cases that the ESS covers and the cost of adding an additional storage module. In this case, SC was considered an appropriate technology for the present application (fast and high number of charge/discharge cycles). It was obtained that four cabinets was the most "optimal" value with a percentage of usage in all of them greater than 33%, although with just three cabinets 80% of power compensation was achieved.

The dimensioning process was more restricting in terms of energy, obtaining, and excess of power capability. By either considering three or four SC cabinets to compensate the power oscillation, there was an excess of power. That was already identified in Figure 14b, where the fact that the line representing the storage technology was quite far from the curves knee. As a consequence, and although in this case it was initially selected SC as technology for available space and economic reasons, it would be interesting to explore other solutions such as flywheels, with a much better ratio energy/power for this application or even a hybrid storage system should not be disregarded.

　　　　Finally, it should be highlighted that this methodology can be applied to different renewable generation plants (solar, wind, etc.) connected to the grid that have to comply with grid code standards of different countries or regions.

Author Contributions: Conceptualization, G.N., J.N. and M.B.; methodology, J.T. and M.B.; software, M.B. and Á.S.; validation, G.N. and Á.S.; formal analysis, G.N. and J.T.; investigation, G.N.; data curation, M.B. and M.S.-H.; writing—original draft preparation, G.N. and J.N.; writing—review and editing, M.L., D.R. and G.N.; visualization, G.N. and M.S.-H.; supervision, M.L. and D.R. All authors have read and agreed to the published version of the manuscript.

Conflicts of Interest: The authors declare no conflict of interest.

References

1.　Robles, E.; Haro-Larrode, M.; Santos-Mugica, M.; Etxegarai, A.; Tedeschi, E. Comparative analysis of European grid codes relevant to offshore renewable energy installations. *Renew. Sustain. Energy Rev.* **2019**, *102*, 171–185. [CrossRef]

2.　Cruz, J. *Ocean Wave Energy*; Springer Berlin Heidelberg: Berlin, Germany, 2008.

3.　Villalba, I.; Blanco, M.; Pérez-Díaz, J.I.; Fernández, D.; Díaz, F.; Lafoz, M.; Perez-Diaz, J.I.; Fernandez, D.; Díaz, F. Wave farms grid code compliance in isolated small power systems. *IET Renew. Power Gener.* **2019**, *13*, 171–179. [CrossRef]

4.　Aderinto, T.; Li, H. Ocean Wave Energy Converters: Status and Challenges. *Energies* **2018**, *11*, 1250. [CrossRef]

5.　Lehmann, M.; Karimpour, F.; Goudey, C.A.; Jacobson, P.T.; Alam, M.R. Ocean wave energy in the United States: Current status and future perspectives. *Renew. Sustain. Energy Rev.* **2017**, *74*, 1300–1313. [CrossRef]

6.　Khojasteh, D.; Mousavi, S.M.; Glamore, W.; Iglesias, G. Wave energy status in Asia. *Ocean Eng.* **2018**, *169*, 344–358. [CrossRef]

7.　Drew, B.; Plummer, A.R.; Sahinkaya, M.N. A review of wave energy converter technology. *Proc. Inst. Mech. Eng. Part A J. Power Energy* **2009**, *223*, 887–902. [CrossRef]

8.　Al-Shetwi, A.Q.; Hannan, M.A.; Jern, K.P.; Mansur, M.; Mahlia, T.M.I. Grid-connected renewable energy sources: Review of the recent integration requirements and control methods. *J. Clean. Prod.* **2020**, *253*, 119831. [CrossRef]

9.　Eltigani, D.; Masri, S. Challenges of integrating renewable energy sources to smart grids: A review. Renew. Sustain. *Energy Rev.* **2015**, *52*, 770–780.

10.　Blanco, M.; Navarro, G.; Lafoz, M.; Perez, J.I. Study of the impact of wave energy generation in the frequency of an island electric grid. In Proceedings of the 12th European Wave and Tidal Energy Conference (EWTEC), Cork, Ireland, 27 August–1 September 2017.

11.　Blavette, A.; O'Sullivan, D.L.; Alcorn, R.; Lewis, T.W.; Egan, M.G. Impact of a medium-size wave farm on grids of different strength levels. *IEEE Trans. Power Syst.* **2014**, *29*, 917–923. [CrossRef]

12.　Macdowell, J.; Wang, Y.; Quint, R.; Chi, Y.; Ernst, B.; Saylors, S.; Jacobson, D.; Andresen, B.; Sorensen, P.E.; Portales, R.; et al. A journey through energy systems integration: Trending grid codes, standards, and IEC collaboration. *IEEE Power Energy Mag.* **2019**, *17*, 79–88. [CrossRef]

13.　Wu, Y.K.; Chang, S.M.; Mandal, P. Grid-connected wind power plants: A survey on the integration requirements in modern grid codes. In Proceedings of the Conference Record—Industrial and Commercial Power Systems Technical Conference, Calgary, AB, Canada, 5–8 May 2019; pp. 1–9. [CrossRef]

14.　Karbouj, H.; Rather, Z.H. A Comparative Study on the Impact of Grid Code Regulations on Stability of Wind Integrated Power Systems. In Proceedings of the 2019 IEEE 1st Global Power, Energy and Communication Conference, GPECOM 2019, Nevsehir, Turkey, 12–15 June 2019; Institute of Electrical and Electronics Engineers Inc.: New York, NY, USA, 2019; pp. 342–347.

15.　Karray, I.; Ben Kilani, K.; Elleuch, M. Wind Plant Control under Grid Code Requirements. In Proceedings of the 16th International Multi-Conference on Systems, Signals and Devices, SSD 2019, Istanbul, Turkey, 21–24 March 2019; Institute of Electrical and Electronics Engineers Inc.: New York, NY, USA, 2019; pp. 706–711.

16.　Attya, A.B. Provision of frequency support by wind power plants: Assessment of compliance with grid codes. In Proceedings of the 2019 IEEE Milan PowerTech, PowerTech 2019, Milan, Italy, 23–27 June 2019; Institute of Electrical and Electronics Engineers Inc.: New York, NY, USA, 2019; p. 8810978.

17.　Lin, D.; Li, X.; Ding, S. An Investigation on Cost-effectiveness of Photovoltaic Power Ramp Rate Control by Using the Levelized Cost of Electricity. In Proceedings of the Asia-Pacific Power and Energy Engineering Conference (APPEEC), Nanjing, China, 20–23 September 2020; pp. 1–6. [CrossRef]

18.　Coe, R.G.; Bacelli, G.; Wilson, D.G.; Abdelkhalik, O.; Korde, U.A.; Robinett, R.D. A comparison of control strategies for wave energy converters. *Int. J. Mar. Energy* **2017**, *20*, 45–63. [CrossRef]

19.　Hong, Y.; Waters, R.; Boström, C.; Eriksson, M.; Engström, J.; Leijon, M. Review on electrical control strategies for wave energy converting systems. *Renew. Sustain. Energy Rev.* **2014**, *31*, 329–342. [CrossRef]

20.　Li, L.; Yuan, Z.; Gao, Y.; Zhang, X. Wave Force Prediction Effect on the Energy Absorption of a Wave Energy Converter With Real-Time Control. *IEEE Trans. Sustain. Energy* **2019**, *10*, 615–624. [CrossRef]

21.　Göteman, M.; Engström, J.; Eriksson, M.; Isberg, J.; Leijon, M. Methods of reducing power fluctuations in wave energy parks. J. Renew. *Sustain. Energy* **2014**, *6*, 043103.

22.　Chabane, S.B.; Alamir, M.; Fiacchini, M.; Riah, R.; Kovaltchouk, T.; Bacha, S. Electricity Grid Connection of a Tidal Farm: An Active Power Control Framework Constrained to Grid Code Requirements. *IEEE Trans. Sustain. Energy* **2018**, *9*, 1948–1956. [CrossRef]

23.　Zhou, Z.; Benbouzid, M.; Frédéric Charpentier, J.; Scuiller, F.; Tang, T. A review of energy storage technologies for marine current energy systems. *Renew. Sustain. Energy Rev.* **2013**, *18*, 390–400. [CrossRef]

24.　Chauhan, A.; Saini, R.P. A review on Integrated Renewable Energy System based power generation for stand-alone applications: Configurations, storage options, sizing methodologies and control. *Renew. Sustain. Energy Rev.* **2014**, *38*, 99–120. [CrossRef]

25.　Anwar, M.B.; El Moursi, M.S.; Xiao, W. Novel Power Smoothing and Generation Scheduling Strategies for a Hybrid Wind and Marine Current Turbine System. *IEEE Trans. Power Syst.* **2017**, *32*, 1315–1326. [CrossRef]

26.　Wu, F.; Zhang, X.P.; Ju, P. Application of the Battery Energy Storage in Wave Energy Conversion system. In Proceedings of the 1st International Conference on Sustainable Power Generation and Supply, SUPERGEN 09, Nanjing, China, 6–7 April 2009.

27.　Rojas-Delgado, B.; Alonso, M.; Amaris, H.; de Santiago, J. Wave Power Output Smoothing through the Use of a High-Speed Kinetic Buffer. *Energies* **2019**, *12*, 2196. [CrossRef]

28.　Rajapakse, G.; Jayasinghe, S.; Fleming, A.; Negnevitsky, M. Grid Integration and Power Smoothing of an Oscillating Water Column Wave Energy Converter. *Energies* **2018**, *11*, 1871. [CrossRef]

29.　Rajapakse, G.; Jayasinghe, S.; Fleming, A. Power management of an oscillating water column wave energy converter with battery/supercapacitor hybrid energy storage. In Proceedings of the 2018 8th International Conference on Power and Energy Systems, ICPES 2018, Colombo, Sri Lanka, 21–22 December 2018; Institute of Electrical and Electronics Engineers Inc.: New York, NY, USA, 2019; pp. 246–251.

30.　Moreno-Torres, P.; Blanco, M.; Navarro, G.; Lafoz, M. Power smoothing system for wave energy converters by means of a supercapacitor-based energy storage system. In Proceedings of the 2015 17th European Conference on Power Electronics and Applications (EPE'15 ECCE-Europe), Geneva, Switzerland, 8–10 September 2015; Institute of Electrical and Electronics Engineers Inc.: New York, NY, USA, 2015.

31.　Agarwal, A.; Iyer, V.M.; Anurag, A.; Bhattacharya, S. Adaptive control of a hybrid energy storage system for wave energy conversion application. In Proceedings of the 2019 IEEE Energy Conversion Congress and Exposition (ECCE), Baltimore, MD, USA, 29 September–3 October 2019; Institute of Electrical and Electronics Engineers Inc.: New York, NY, USA, 2019; pp. 4994–5001.

32.　Rasool, S.; Muttaqi, K.M.; Sutanto, D. Modelling of a wave-to-wire system for a wave farm and its response analysis against power quality and grid codes. *Renew. Energy* **2020**, *162*, 2041–2055. [CrossRef]

33.　Tedeschi, E.; Santos-Mugica, M. Modeling and control of a wave energy farm including energy storage for power quality enhancement: The bimep case study. *IEEE Trans. Power Syst.* **2014**, *29*, 1489–1497. [CrossRef]

34.　Yan, Z.; Zhang, X.P. Adaptive energy filters smoothing renewable power fluctuations at different power levels. In *IET Conference Publications*; Institution of Engineering and Technology: London, UK, 2019; Volume 2019.

35.　Kovaltchouk, T.; Multon, B.; Ahmed, H.B.; Aubry, J.; Venet, P. Enhanced aging model for supercapacitors taking into account power cycling: Application to the sizing of an energy storage system in a direct wave energy converter. In Proceedings of the 2014 9th International Conference on Ecological Vehicles and Renewable Energies (EVER), Monte-Carlo, Monaco, 25–27 March 2014; pp. 1–10. [CrossRef]

36.　Torres, J.; Moreno-Torres, P.; Navarro, G.; Blanco, M.; Lafoz, M. Fast Energy Storage Systems Comparison in Terms of Energy Efficiency for a Specific Application. *IEEE Access* **2018**, *6*, 40656–40672. [CrossRef]

37.　Energías Marinas—EVE. Available online: https://eve.eus/Actuaciones/Marina?lang=es-es (accessed on 4 February 2021).

38.　Electric Double Layer Capacitor—An Overview. Electric Double Layer Capacitor—An Overview | ScienceDirect Topics. Available online: https://www.sciencedirect.com/topics/engineering/electric-double-layer-capacitor (accessed on 5 January 2021).

39.　*International Electrotechnical Commission Electrical Energy Storage—White Paper*; International Electrotechnical Commission: Geneva, Switzerland, 2011; pp. 1–78.

40.　Grbović, P. Ultra-Capacitor Energy Storage Devices. In *Ultra-Capacitors in Power Conversion Systems*; John Wiley & Sons, Ltd.: Hoboken, NJ, USA, 2013; pp. 22–77.

41.　Rafik, F.; Gualous, H.; Gallay, R.; Crausaz, A.; Berthon, A. Frequency, thermal and voltage supercapacitor characterization and modeling. *J. Power Sources* **2007**, *165*, 928–934. [CrossRef]

42.　Chaoui, H.; Gualous, H. Online Lifetime Estimation of Supercapacitors. *IEEE Trans. Power Electron.* **2017**, *32*, 7199–7206. [CrossRef]

43.　Mohan, N.; Undeland, T.; Robbins, R. *Power Electronics Converters, Applications and Design*; John Wiley & Sons: Hoboken, NJ, USA, 1995.

44.　Navarro, G.; Nájera, J.; Torres, J.; Blanco, M.; Santos, M.; Lafoz, M. Development and Experimental Validation of a Supercapacitor Frequency Domain Model for Industrial Energy Applications Considering Dynamic Behaviour at High Frequencies. *Energies* **2020**, *13*, 1156. [CrossRef]

45. Maxwell Technologies Maxwell Technologies Ultracapacitors, Supercapacitors, Microelectronics and High Voltage. Available online: https://www.maxwell.com/ (accessed on 10 February 2021).
46. Zuo, X.; Li, G.Z. Isolated voltage balancing in super-capacitor energy storage system. In Proceedings of the 26th Chinese Control and Decision Conference (CCDC), Changsha, China, 31 May–2 June 2014; IEEE Computer Society: Washington, DC, USA, 2014; pp. 5124–5128.
47. Li, L.; Huang, Z.; Liu, W.; Li, H.; Li, H.; Yang, Y. A controllable voltage equalizer with state of charge prediction for supercapacitors in large current applications. In *IFAC Proceedings Volumes (IFAC-PapersOnline)*; IFAC Secretariat: Laxenburg, 2014; Volume 19, pp. 3623–3628.
48. MATLAB - El Lenguaje del Cálculo Técnico—MATLAB & Simulink. Available online: https://es.mathworks.com/products/matlab.html (accessed on 4 January 2021).
49. Castano, S.; Gauchia, L.; Sanz-Feito, J. Effect of packaging on supercapacitors strings modeling: Proposal of functional unit defined around balancing circuit. *IEEE Trans. Compon. Packag. Manuf. Technol.* **2013**, *3*, 1390–1398. [CrossRef]
50. Zhang, S.; Yu, X. A unified analytical modeling of the interleaved pulse width modulation (PWM) DC-DC converter and its applications. *IEEE Trans. Power Electron.* **2013**, *28*, 5147–5158. [CrossRef]
51. Arango, E.; Ramos-Paja, C.; Calvente, J.; Giral, R.; Serna, S. Asymmetrical Interleaved DC/DC Switching Converters for Photovoltaic and Fuel Cell Applications—Part 1: Circuit Generation, Analysis and Design. *Energies* **2012**, *5*, 4590–4623. [CrossRef]
52. BiMEP BiMEP Mutriku. Available online: https://www.bimep.com/area-mutriku/servicios/ (accessed on 10 February 2021).
53. Blanco, M.; Navarro, G.; Lafoz, M.; Pérez, J.I. How harmful is the wave energy penetration in an electric grid? In *Proceedings of the Twelfth European Wave and Tidal Energy Conference*; Lewis, A., Ed.; University College Cork: Cork, Ireland, 2017; p. 942.
54. Lafoz, M.; Blanco, M.; Beloqui, L.; Navarro, G.; Moreno-Torres, P. Dimensioning methodology for energy storage devices and wave energy converters supplying isolated loads. *IET Renew. Power Gener.* **2016**, *10*, 1468–1476. [CrossRef]
55. Moreno-Torres, P.; Lafoz, M.; Navarro, G.; Blanco, M.; García-Tabarés, L. Sistema para el acondicionamiento de la potencia eléctrica generada en un sistema de generación undimotriz. 2016, pp. 1–32. Available online: https://www.patentes-y-marcas.com/fr/brevet/sistema-para-el-acondicionamientode-la-potencia-electrica-generada-en-un-sistema-de-generacion-undimotriz-p201530980 (accessed on 5 January 2021).
56. Lafoz, M.; Blanco, M.; Ramirez, D. Grid connection for wave power farms. In Proceedings of the 2011 14th European Conference on Power Electronics and Applicationsm, Birmingham, UK, 30 August–1 September 2011; IEEE: New York, NY, USA, 2011; pp. 1–10.
57. *ENTSO-E European Network of Transmission System Operators for Electricity (ENTSO-E)*; European Union: Brussels, Belgium, 2016.
58. EASE. *EERA European Energy Storage Technology Development Roadmap - 2017*; EERA: Brussels, Belgium, 2017.
59. Gatta, F.M.; Geri, A.; Lauria, S.; Maccioni, M.; Palone, F. Battery energy storage efficiency calculation including auxiliary losses: Technology comparison and operating strategies. In Proceedings of the 2015 IEEE Eindhoven PowerTech, Eindhoven, The Netherlands, 29 June–2 July 2015.
60. Funaki, T. Evaluating energy storage efficiency by modeling the voltage and temperature dependency in EDLC electrical characteristics. *IEEE Trans. Power Electron.* **2010**, *25*, 1231–1239. [CrossRef]